Oral Candidacy Exam proposal:
Dated 19th of March, 2017

A search for Lepton Flavor Violating Decays of the Higgs Boson

Nabarun Dev[a]

[a] *Department of physics, University of Notre Dame, Indiana, USA*

E-mail: nabarun.dev@cern.ch, ndev@nd.edu

Abstract: A proposal is presented here outlining the search for lepton flavor violating (LFV) decays of the Higgs boson using the CMS experiment at the LHC. This a search for physics beyond the standard model and is performed with events where the Higgs decays to a muon and a tau lepton with the tau further decaying to an electron. The signal for which we are searching, the backgrounds and the experimental techniques used to discrimate signal from background are outlined in this proposal.

1 Introduction

The Standard Model (SM) of particles physics is the most well-tested and elegant description of nature available today. The discovery of the Higgs Boson in 2012 [1] added another feather in the hat of the SM. In the SM, elementary particles acquire mass from their interaction with the scalar Higgs field, the quantum of which is the Higgs Boson. Besides confirming the above mechanism by which particles acquire mass, the above discovery is also significant beause the Higgs provides a portal for us to not only further study the processes within the SM, but also to look for new physics processes beyond it (BSM). One of the main goals of the LHC physics programme at CERN is to search for such BSM processes.

Lepton flavour violating (LFV) interactions between charged leptons cannot naturally occur within the standard model and such a process has never been observed experimentally. However, such decays are allowed in many BSM theories such as models with more than one Higgs doublet [2], supersymmetric models [3] and many others. Such interactions could thus be an indicator of new physics and could be realized in decays of the Higgs Boson into two charged leptons of different flavor. Indirect constraints on LFV Higgs decays exists through interpretations of measurements of processes such as $\tau \to \mu\gamma; \mu \to e\gamma$ [4] [5]. These constraints set weak limits on LFV Higgs decays allowing significant branching fractions;$Br(H \to \mu\tau) < O(10\%)$. A search for $H \to \mu\tau$ performed with data collected by the CMS during run I of the LHC improved the above limits by an order of magnitude to $Br(H \to \mu\tau) < O(1.51\%)$. at 95% confidence level. Also, an excess of events with a significance of 2.4σ was observed. This warrants us to do this search with much larger

amount of data which would either lead us to confirm this excess or squash it and set much stricter limits on this process. The run II of LHC (see section **??**) provides us with such an opportunity to perform the search outlined in the following.

2 LHC and the CMS

The Large Hadron Collider (LHC) is a circlar particle accelerator designed to collide proton beams with a centre-of-mass energy of 14 TeV. It consists of a 27-kilometre ring of superconducting magnets with a number of accelerating structures to boost the energy of the particles along the way. Currently, (run II) the LHC operating at a COM energy of 13 TeV (compared to 7 TeV in run I) and luminosities up to $1.5 \times 10^{34}\text{cm}^{-2}\text{s}^{-1}$. Under run II conditions, the Higgs production cross-section is a factor 2 higher [6] than run I (see figure **??**) and almost twice the amount of dta has already been collected.

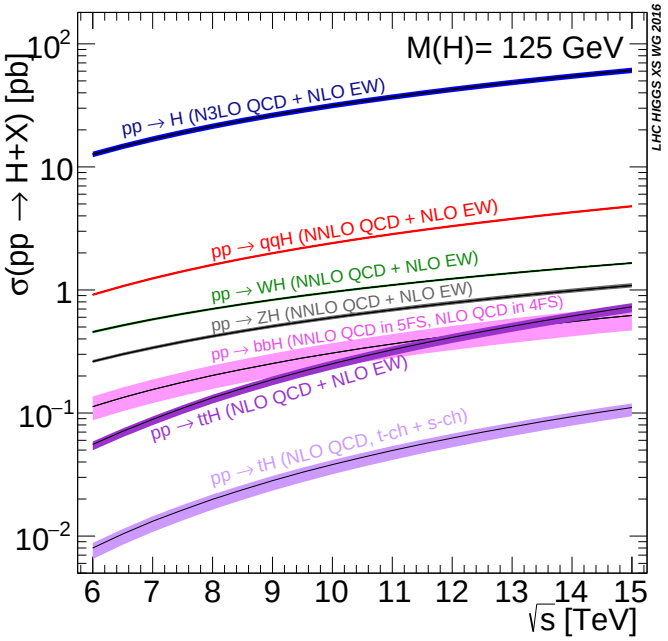

Figure 1. Higg production cross-section as a function of the collison center-of-mass energy

The Compact Muon Solenoid (CMS) is a large general purpose particle physics detector designed to study proton-proton collisions produced by LHC. A detailed description of the CMS detector can be found here [7]. I consists of a super conducting solenoid that houses tracking and calorimetry systems and provides an axial magnetic field of 3.8T.The inner-most layer is the silicon pixel and strip tracker that measures the trajectories of charge particles and covers a range of $|\eta| < 2.5$(η is the pseudorapidity defined as $-ln[tan(\frac{\theta}{2})]$, where θ is polar angle of the particle's trajectory with respect to the beam direction). Surrounding the tracker are lead tungstate crystal electromagnetic calorimeter (ECAL) which measures the energy of electrons and photons, and the hadronic calorimeter (HCAL) which measure the energy of heaviour particles that pass through the HCAL. The ECAL also contains preshower detector for extra spatial precision.Surrounding

the solenoid is the muon system which has gas-ionization detectors placed in the steel yoke of the magnet. This isthe outermost component of CMS and measures the momenta of muons that traverse through it. Only a small fraction of events produced by the LHC can be permanently stored, and to select these events of interest, CMS employs a sophisticated two-level trigger system, organized in two consecutive stages- the Level-1 (L1) trigger and the High Level Trigger (HLT). The L1 trigger is implemented using custom hardware and makes decisions based on coarse information from the calorimeters and the muon systems, reducing the rate from 40 MHz to 100 kHz. It has a latency of 3.8μs. The software-based HLT partially reconstructs the event, implementing complex selection algorithms on finer granularity information from all sub-detectors in regions deemed interesting by the L1 decision. It runs on a massive computer farm and brings down the rate further to less than 1.5 kHz. I am part of a team that works on the cusp of ECAL and L-1 trigger and have helped maintain and improve the functioning of this system. This is mentioned in detail in section 1.

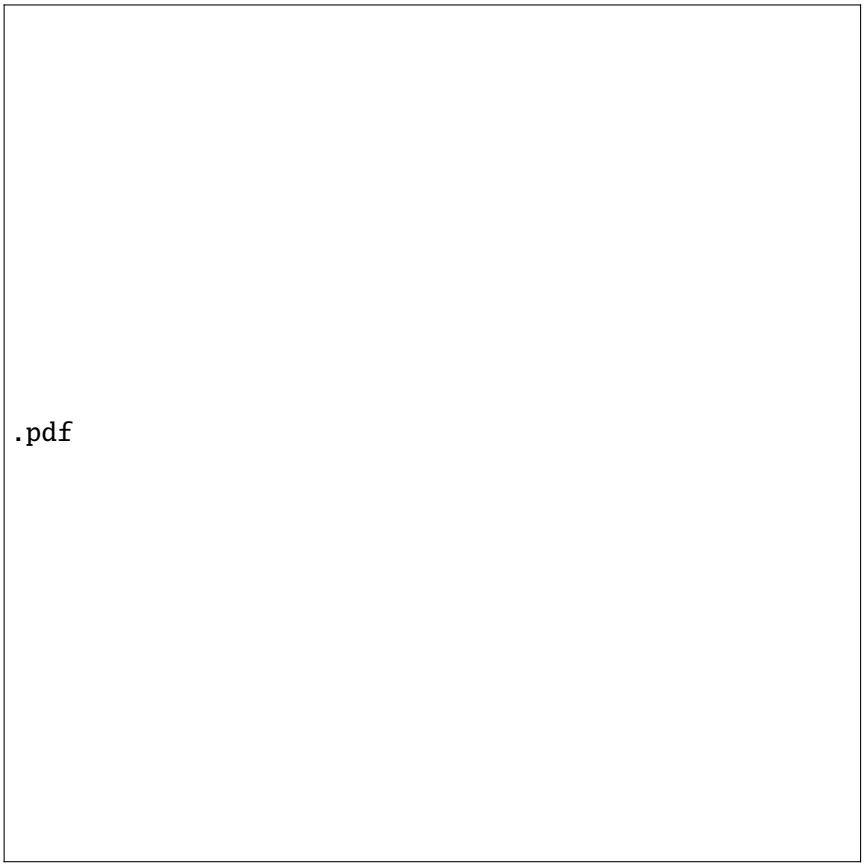

Figure 2. The upgraded trigger architecture. The layers of the calorimeter trigger are seen on the left. The different layers of the muon trigger system are shown on the right. The global trigger combines information from both systems to form the Level-1 decision.

2.0.1 Upgraded trigger architecture

The L1 trigger upgrade has benefitted immensely from recent technological developments. New optical link boards for the ECAL and HCAL with speeds ranging from 4.8 Gb/s to 6.4 Gb/s have

replaced the existing copper cables (1.2 Gb/s). The TMT architecture is based on recent μTCA electronics standard and is comprised of two processing layers formed by custom made Advanced Mezzanine Cards equipped with powerful Xilinx Virtex-7 FPGAs. The layer-1, designed for data formatting and preprocessing, is comprised of 18 CTP7 (Calorimeter Trigger Processor) cards that receive data from different sections of the ECAL, HCAL (hadronic calorimeter) and HF (hadronic forward calorimeter). The layer-2 is the main processing layer and is comprised of 9 MP7 (Master Processor) cards as shown on Figure 2. These cards hold the algorithms and have access to the entire calorimeter information (sent from all layer-1 cards) on single FPGAs.

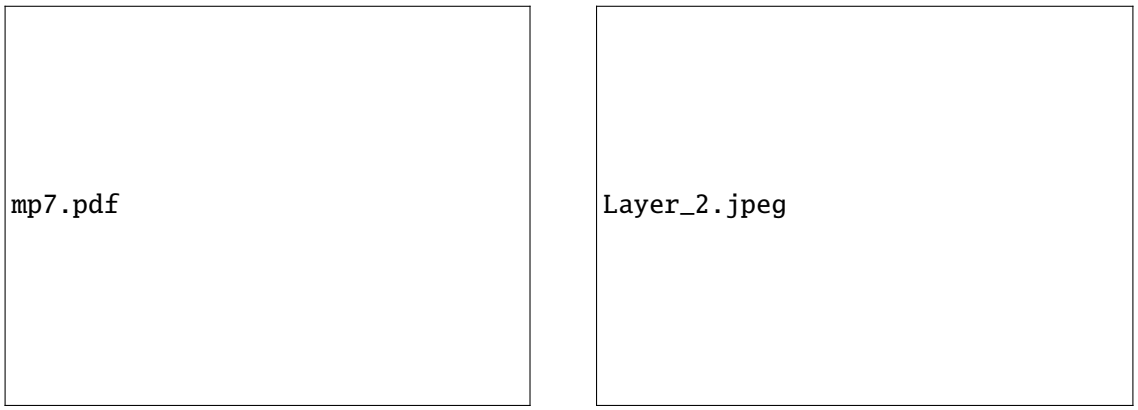

Figure 3. A MP7 card (left), the main processing unit of Level-1 calorimeter trigger and a photo of the layer-2 crate that houses the MP7 cards (right) .

All data for a given BX is sent by the 18 layer-1 cards to a layer-2 card. Data from subsequent BXs are sent to different layer-2 cards. This proceeds until the first card has finished processing and is ready to receive data again. The data thus processed by layer-2 cards is sent to the global trigger which takes the final L1 decision after combining the calorimeter data with information from the muon systems.

3 Improved electron and photon trigger algorithm

The primary aim of the L1 algorithms is to reach a performance level comparable to offline reconstruction algorithms, or to get as close as possible. Since the L1 trigger is a synchronous electronic system, all algorithms implemented in the firmware must have fixed latency. Offline reconstruction algorithms, on the other hand, are typically iterative. The upgraded L1 trigger employs newly-developed sophisticated algorithms for reconstructing electrons and photons. No tracker information is available at Level-1 making electrons and photons indistinguishable at this stage. By thoroughly exploiting the advantages offered by the new hardware architecture, as described below, these algorithms have provided several improvements with respect to previous electron and photon reconstruction [7]. These include better position and energy reconstruction, better identification of e/γ candidates, more precise isolation criteria and a reduction in triggering rate.

3.1 Description of the new e/γ algorithms

An improved energy containment and energy reconstruction is achieved via dynamic clustering. This technique replaces previous sliding window techniques and is the first time dynamic clustering has been introduced in the Level-1 firmware. The local energy maximum above a fixed threshold, as shown in red in Figure 3, is designated as the seed tower. Clusters of towers are then built from a seed tower with the first and second neighbors dynamically clustered together with the seed. An extended region in the ϕ-direction (up to 5 TTs) helps recover energy lost due to bremsstrahlung. This is particularly important in the case of showering electrons and converted photons. However, only a narrow region (at most 2 TTs) is allowed in the η-direction because electromagnetic showers are compact and generally do not spread over more than 2 TTs in η. The maximum size of clusters is limited to 8 TTs in order to minimize the impact of pileup energy deposits. The sum of the transverse energy recorded in the ECAL of all the towers in the cluster is the raw cluster E_T.

The position reconstruction of e/γ candidates has been also improved by exploiting the tower level granularity. Starting from the center of the seed tower, the position of the cluster is refined within the seed, using the distribution of the energy in the cluster to construct an energy-weighted average. These new algorithms also take advantage of many cluster shapes produced by dynamic clustering that depend on the energy distribution around the seed tower as displayed in Figure 3 (right). Some large cluster shapes are very unlikely to be associated with electrons/photons and likely come from jets. Electron/photon clusters are typically smaller, containing at most four TTs. This provides discriminating power for e/γ identification. In addition to the cluster shapes, the energy distribution within the crystals of a seed tower (fine grain veto bit) and ratio of energy deposited in ECAL and HCAL seed towers are also used to obtain better identification of electrons and photons.

3.2 Energy calibration and isolation criteria for e/γ candidates

Two layers of calibrations are applied at Level-1. The first set of calibrations is applied at layer-1. They are applied at the trigger tower level and are hence common for all downstream objects. To derive them for the ECAL, a single π^0 Monte-Carlo (MC) dataset without pileup was used. The corrections were obtained by comparing the generator level value of the pion energy deposit to the TP, and they depend on η and the transverse energy of the TP. These calculations were later repeated on Run II 13 TeV data. Corrections for HCAL were derived in a similar way using a single charged pion MC without pileup. A second layer of calibrations are applied at layer-2 at the e/γ object level. They are applied on the raw E_T of a e/γ cluster (see section 2.1) in order to be similar to the E_T of the e/γ candidates reconstructed offline. These corrections have been obtained by comparing the E_T of the Level-1 e/γ clusters to the E_T of corresponding fully reconstructed offline electron candidates in Run II 13 TeV data, using $Z \rightarrow ee$ events with tag-and-probe selection. They depend on the η-position of the seed tower, the shape of the cluster and the uncalibrated energy of the cluster, and are encoded in a Look-Up-Table (LUT). These corrections provide a uniform energy response throughout the detector and improve the energy resolution.

A more precise isolation criteria has also been implemented exploiting the full detector view that is now available at layer-2. The isolation region, as seen on Figure 3 (left), is defined as 6×9 TT area excluding the e/γ footprint in ECAL (2×5 TT region) and HCAL (1×2 TT region). A

candidate is considered isolated if it has deposited energy in the isolation region that is less than a threshold that depends on pileup, η and raw E_T of the candidate. The level of pileup is estimated, on an event-by-event basis, using the number of TTs in the central region (8 central η rings) of the calorimeter with an energy deposit greater than or equal to 500 MeV. These thresholds were obtained from Run II 13 TeV data, using $Z \rightarrow ee$ events with a tag-and-probe selection. They were calculated such that the efficiency of the isolation criterion is constant as a function of pileup and η, but at the same time increasing with E_T to ensure a 100% efficiency for high ET candidates. The isolation thresholds are flexible and have been retuned as the luminosity of the LHC increased in order to keep the e/γ thresholds low. It is also possible to have several LUTs containing isolation thresholds for different luminosity ranges.

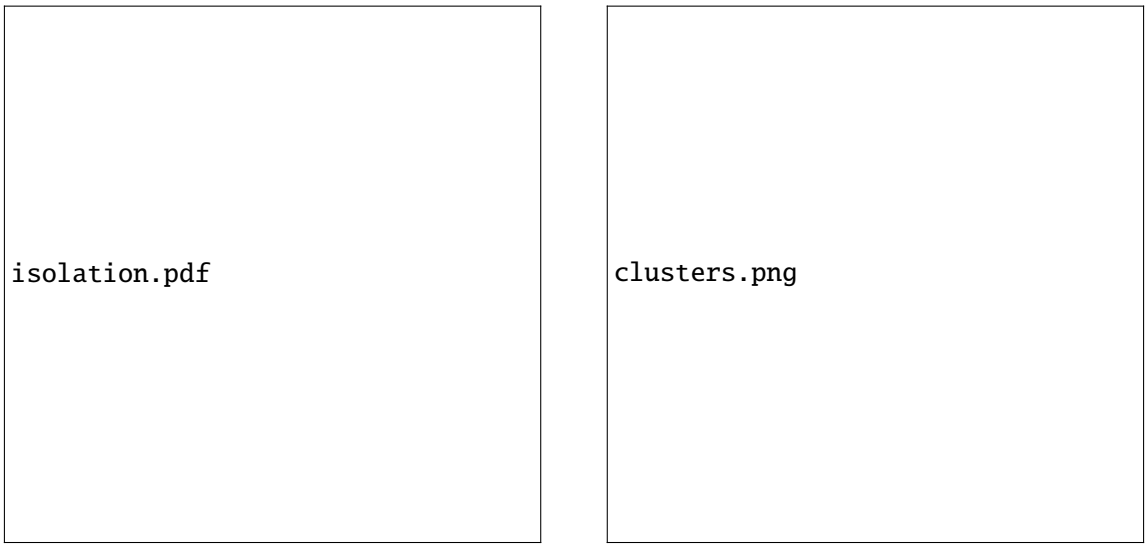

Figure 4. Left: Illustration of dynamic clustering of TTs and e/γ isolation region (blue) with the exclusion of footprints in ECAL and HCAL. Right: Various cluster shapes from dynamic clustering. Smaller e/γ-like clusters are shown on top and larger jet like clusters are shown below.

These algorithms were developed using Run I data and simulated Run II data. Their performance was then validated using data taken in 2015 during the commissioning period of the new trigger system, and they exhibit much superior performance compared to the Run I trigger. The position resolution is better by a factor of 4 and the energy resolution has improved by up to 30% with respect to Run I [8]. In particular, the energy resolution in the EE is now improved and closer to that in the EB. This is due to dynamic clustering being very well adapted to the complex geometry of EE. Further, the efficiency is also better with sharper turn-on curves accompanied by a reduction in rate.

3.3 Firmware implementation

The algorithms are implemented in the firmware using the VHDL hardware description language. The firmware for the electron finder along with the tau lepton and jet finders must fit within a single Xilinx FPGA, which makes its implementation a challenge. In addition, the core firmware, which comprises all necessary logic to control the I/O optical serial links, the configuration registers, the

input pattern buffers, output spy buffers are also included. As seen in Figure 4, a precise floor planning scheme was developed to efficiently perform a place and route process, and to guarantee that timing constraints are satisfied after modification of VHDL sources during the development process. An internal processing speed of 240 MHz has been achieved with this approach. About 65% of the logic resources of the chip are being used, which include the electron/photon, jet, tau lepton and missing E_T triggers. The software interface is based on the IPBUS standard using libraries such as μHAL developed at CERN [5]. The TMT architecture allows for data coming from

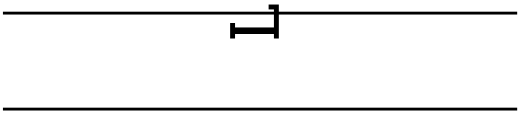

Figure 5. Floor planning of Xilinx Virtex 7 FPGA within the MP7 board. The purple areas represent the input-output logic within the core firmware and the yellow represents the resources used by the algorithms. The red corresponds to the DAQ interface and the green the IPBus that handles the communications.

calorimeters to be rearranged in geometrical order [6]. Algorithms are fully pipelined (spatially) and process data at the incoming rate starting on the reception of the first data word. The TTs are combined to form basic blocks of 3×1 TTs (see section **??**) upon reception. These are further combined to form bigger blocks which are the input components of algorithms. Potential cluster seeds are identified depending on the TT energy threshold. Quality flags are also set for each incoming TT based on several predefined selection criteria and help in reducing the number of resources required for the implementation of lepton cluster logic. The fully pipelined firmware approach provides an efficient way to localize the processing, reduce the size and number of fan-outs, minimize routing delays and eliminates register duplication leading to a compact and easily maintainable firmware.

4 Performance of the upgraded e/γ trigger in 2016

The new L1 trigger system was commissioned in September 2015 and has been used for physics throughout data taking in 2016, and has delivered very good performance from the start. Its performance has remained excellent with the LHC delivering data at increasingly higher luminosities with higher pileup levels. The performance of the trigger in 2016 CMS physics data taking is shown in Figures 5, 6 and 7. The position resolution of the new trigger system in 2016 is presented in Figure 5. This was computed with respect to offline electron superclusters (these are clusters produced by offline electron reconstruction algorithms) using $Z \rightarrow ee$ events in 13 TeV data recorded in 2016. These plots illustrate excellent spatial resolution provided by the new trigger. The energy resolution of the L1 trigger is shown in Figure 6. This was computed with respect to transverse energy of the offline electron superclusters using $Z \rightarrow ee$ events. A geometrical matching between the electron supercluster and the L1 candidate is applied. The energy resolution delivered is excellent in all η ranges. In terms of trigger efficiency, turn-on curves for 2016 $Z \rightarrow ee$

data, evaluated using tag-and-probe techniques are shown in Figure 7. The sharp turn-on curves and high trigger efficiency are due to the excellent energy resolution and the performance of the new clustering algorithms. These sharp turn-on curves allow CMS to maintain low thresholds on physics object selection.

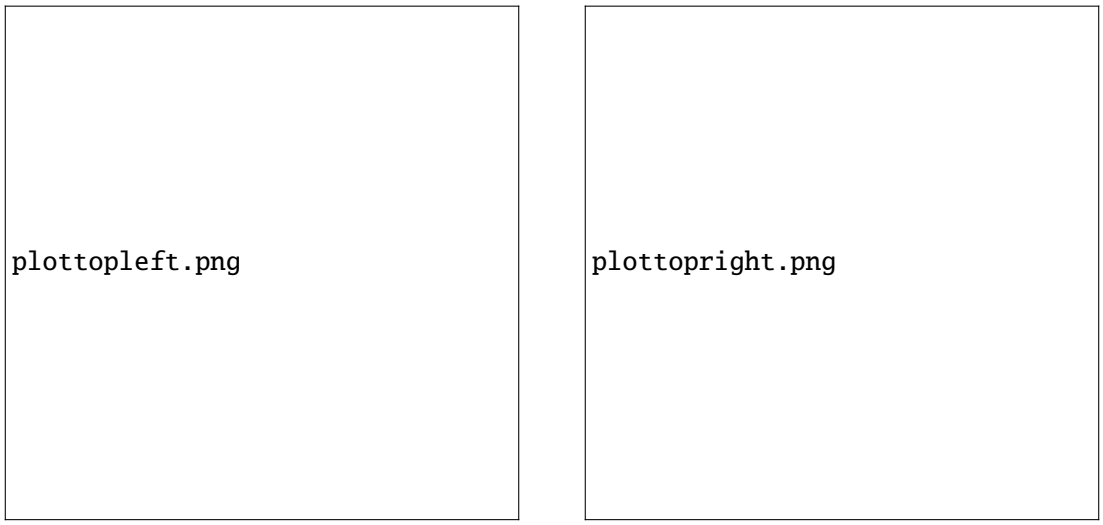

Figure 6. Differences in pseudo-rapidity η (left) and azimuthal angle ϕ (right) for L1 EG candidates with respect to the offline reconstructed electron supercluster, in the barrel ($|\eta|$<1.479, in black) and in the endcaps ($|\eta|$ >1.479, in red)

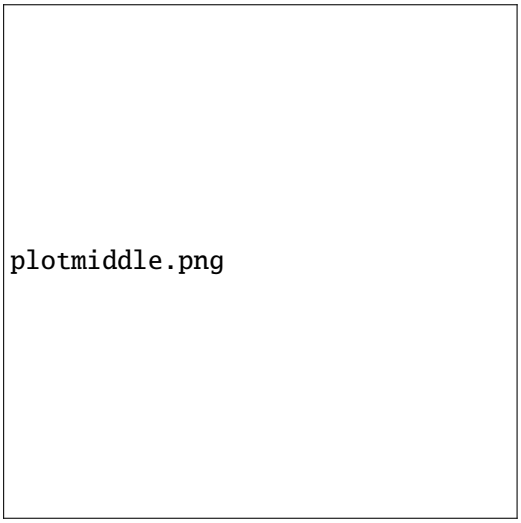

Figure 7. Relative difference in transverse energy for L1 EG candidates with respect to the offline reconstructed transverse energy, in the range $0 \leq |\eta| < 0.25$ (black), $1 \leq |\eta| < 1.25$ (red) and $2 \leq |\eta| < 2.25$ (blue)

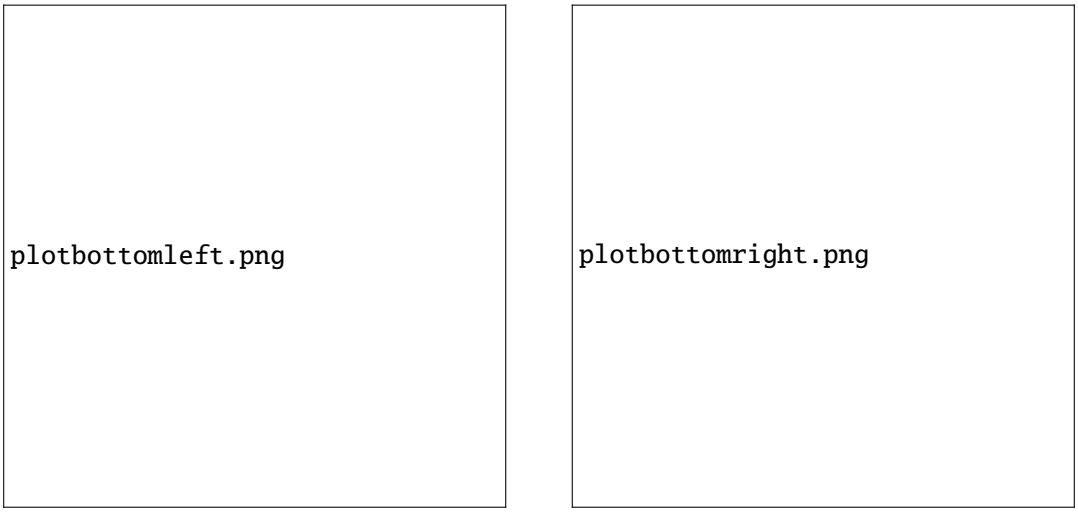

Figure 8. Left: L1 trigger efficiency for an e/γ object as a function of the offline reconstructed supercluster transverse energy E_T for electrons in the barrel ($|\eta|$<1.479, in black) and in the endcaps ($|\eta|$>1.479, in red), for a threshold of 24 GeV (left) with and for a threshold of 40 GeV (right) without isolation requirement.

5 Conclusions

The upgraded calorimeter trigger has been running smoothly from the start of data taking in 2016 and has exhibited excellent performance. The isolation criteria and energy calibration are optimized at regular intervals to follow the increasing LHC luminosity which currently peaks at more than $1.5 \times 10^{34}\text{cm}^{-2}\text{s}^{-1}$. The new trigger has enabled CMS to maintain low e/γ thresholds throughout LHC Run II. The current trigger scheme for physics includes: single isolated and non-isolated e/γ triggers for electroweak (EWK) processes; double e/γ, triple e/γ triggers for Higgs physics. It is possible for CMS to increase its selectivity by introducing new invariant mass triggers for EWK processes. The new trigger architecture, being modular, provides the flexibility to add more processing nodes if needed. It is very important for the e/γ trigger to be able to perform efficiently to be maximally sensitive to new physics signatures over a wide range of particle energies. The new CMS Level-1 electron and photon trigger has delivered very high performance in 2016, consistent with expectations and is expected to do so throughout challenging conditions of LHC Run II and Run III.

References

[1] CMS Collaboration, *The CMS Experiment at the CERN LHC*, *JINST* **3 S08004** (2008) .

[2] CMS Collaboration, *CMS TriDAS project: Technical Design Report, vol. 1: The Trigger Systems* , *CERN-LHCC-2000-038*, **CMS-TDR-6-1** (2000) .

[3] CMS Collaboration, *CMS Technical Design Report for The Level-1 Trigger Upgrade*, *CERN-LHCC-2013-011* **CMS-TDR-12** (2008).

[4] A. Zabi for CMS collaboration*The CMS Level-1 Calorimeter Trigger for LHC Run II*, *these proceedings* **TWEPP** (2016).

[5] T. Williams et al., *IPbus: A flexible Ethernet-based control system for xTCA hardware*, *JINST* **10** **C02019** (2015).

[6] A. Zabi for CMS Collaboration, *Triggering on electrons, jets and tau leptons with the CMS upgraded calorimeter trigger for the LHC RUN II*, *JINST* **11 C02008** (2016).

[7] J.B. Sauvan for CMS Collaboration *Performance and upgrade of the CMS electron and photon trigger for Run 2*, *J. Phys. Conf. Ser.* **587** (2015) 012021.

[8] T. Strebler for CMS Collaboration, *Level-1 trigger selection of electrons and photons with CMS for LHC Run-II*, *CMS CR* **-2015/220** (2008) .